

# Supersolid of Hardcore Bosons on the Face Centered Cubic Lattice

Takahumi Suzuki and Naoki Kawashima

*Institute for Solid State Physics, University of Tokyo, Kashiwa, Chiba 277-8581*

(Dated: May 25, 2019)

We investigate a supersolid state in hardcore boson models on the face-centered-cubic (FCC) lattice. The supersolid state is characterized by a coexistence of crystalline order and superfluidity. Using a quantum Monte Carlo method based on the directed-loop algorithm, we calculate static structure factors and superfluid density at finite temperature, from which we obtain the phase diagram. The supersolid phase exists at intermediate fillings between a three-quarter-filled solid phase and a half-filled solid phase. We also discuss the mechanism of the supersolid state on the FCC lattice.

PACS numbers: 75.40.Gb; 75.10.Pq; 75.10.Jm

Since the possibility of a supersolid state in  $^4\text{He}$ , where off-diagonal long-range order and crystalline order coexist, was discussed by O. Penrose and L. Onsager [1], search for a supersolid has been one of the most intriguing enterprises in physics. Especially, the solid  $^4\text{He}$  has been well studied theoretically and experimentally as a candidate of supersolid matters. For the  $^4\text{He}$  supersolid, several scenarios and predictions have been made theoretically[2, 3, 4, 5, 6]. However, a number of experiments failed to detect the superfluidity in the solid  $^4\text{He}$ . Recently, characteristic behaviors of superfluidity have been reported in torsional oscillator experiments on the solid  $^4\text{He}$  by E. Kim and M. H. W. Chan[7]. In their measurements, decrease of the resonant period was observed in the low temperature region  $T \leq 100\text{mK}$ . The decrease implies the emergence of non-classical rotational inertia in the solid  $^4\text{He}$ . They concluded that such decrease was a signature of a transition into the supersolid phase.

Bosonic lattice systems are also attractive, because they can be materialized by optical lattices with cold atoms. Indeed, the Bose-Einstein condensation of chromium atoms has been successfully realized in the optical trapping potential[8]. Although the supersolid on the optical lattices has not been observed yet, they are promising as hopeful stages to study the supersolid on the bosonic lattice models.

Conventional approaches to the supersolid on bosonic lattice models were adopted by several researchers[5, 6]. They considered the bosonic-lattice-gas models with infinite on-site repulsions, in which the number of bosons on each site is restricted to one or zero. Under this restriction, the original bosonic-lattice models are mapped onto the  $S=1/2$  XXZ model. They calculated the phase diagrams of this model on the body-centered-cubic lattice using a mean-field approximation and discussed the possibility of the supersolid state. Quite recently, the supersolid state on the triangular lattice has been studied precisely[9, 10, 11, 12, 13] by this approach. From these studies, the phase diagram, the finite temperature transition, and the microscopic pictures of the supersolid on the triangular lattice have been clarified[9, 10, 11, 12]. In other two-dimensional lattice models, the possibility of the supersolid state has been also discussed[14, 15, 16,

17, 18]. However, the issue of the existence of the supersolid phase on three-dimensional cases remains to be studied. It is desirable to elucidate the characteristics of the supersolid in three-dimensional bosonic-lattice models beyond the mean-field results.

In this paper, the supersolid in a three-dimensional bosonic-lattice model is studied by a quantum Monte Carlo method based on the directed loop algorithm[19, 20]. We focus on a hardcore-bosonic model on the face-centered-cubic (FCC) lattice. Cases with the positive hopping amplitude  $t > 0$  and the nearest-neighbor repulsion  $V > 0$  are considered. The model Hamiltonian is defined by

$$\mathcal{H} = -t \sum_{\langle ij \rangle} (b_i^\dagger b_j + h.c.) + V \sum_{\langle ij \rangle} \hat{n}_i \hat{n}_j - \mu \sum_i \hat{n}_i, \quad (1)$$

where  $\mu$  is the chemical potential,  $b_i^\dagger (b_i)$  is the bosonic creation (annihilation) operator, and  $\hat{n}_i = b_i^\dagger b_i$ . The summation  $\langle ij \rangle$  is taken over the nearest neighbor pairs and the system size is defined by  $N = L^3$ . The periodic boundary condition is applied. Since the Hamiltonian (1) has a particle-hole symmetry at a half filling  $n = \langle \hat{n} \rangle = 1/2$  ( $\mu = 6V$ ), we only consider the case  $n \geq 1/2$ . Under the hardcore condition, the original bosonic-lattice model given by the Hamiltonian (1) is mapped onto the  $S = 1/2$  XXZ model in a magnetic field,

$$\mathcal{H} = -J_\perp \sum_{\langle ij \rangle} (S_i^x S_j^x + S_i^y S_j^y) - J_z \sum_{\langle ij \rangle} S_i^z S_j^z - H \sum_i S_i^z, \quad (2)$$

where  $J_\perp = 2t$ ,  $J_z = -V$  and  $H = \mu - 6V$ . Consequently, a half filling  $n = 1/2$  and a full filling  $n = 1$  correspond to the magnetization  $m = 0$  and the saturation magnetization  $m = 1/2$ , respectively.

In the limit  $J_\perp/|J_z| \rightarrow 0$ , the Hamiltonian (2) expresses the antiferromagnetic Ising model on the FCC lattice. The precise  $H$ - $T$  phase diagram at  $J_\perp = 0$  has been already investigated[21, 22, 23]: At  $m = 0$  and a half of the saturation magnetization  $m = 1/4$  (the three-quarter fillings), there appear two solid phases conven-

tionally referred to as AB and  $A_3B$ . The typical spin configurations of the AB and  $A_3B$  phases are shown in Fig. 1. In the AB phase, up-spin layers and down-spin layers are stacked alternately along one of orthogonal axes. On the other hand, in the  $A_3B$  phase, antiferromagnetically ordered layers and ferromagnetically ordered layers are stacked alternately. The phase transition from the AB phase to the  $A_3B$  phase occurs at  $H_{\text{Ising}} = 2|J_z|$  at absolute zero temperature.

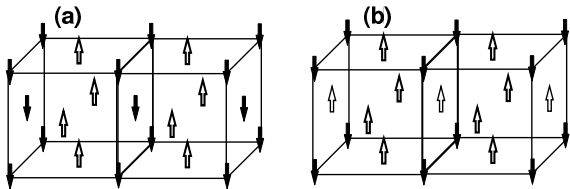


FIG. 1: The two ordered states, (a) AB state and (b)  $A_3B$  state. Note that the lines connecting next-nearest neighbors are no direct couplings.

In order to investigate the crystalline order and the off-diagonal long-range order for  $J_\perp > 0$ , we calculate the static structure factor  $S(\mathbf{Q})$  (SSF) and the superfluid density  $\rho_s$ [24], represented by

$$S(\mathbf{Q}) = \left\langle \left| \sum_i \exp[i\mathbf{Q} \cdot \mathbf{r}_i] \left( S_i^z + \frac{1}{2} \right) \right|^2 \right\rangle \quad (3)$$

and

$$\rho_s = \frac{k_B T \langle \mathbf{W}^2 \rangle}{3J_\perp L}, \quad (4)$$

where  $\mathbf{W} = (W_x, W_y, W_z)$  denotes the winding number.

In what follows, we express the wave vector  $\mathbf{Q}$  by a conventional choice of the unit reciprocal vectors. According to the expressions (3), when the AB or  $A_3B$  ordered state appears in the ground state, strong system-size dependence emerges only at  $\mathbf{Q}_{\text{sol}} = (\pi, \pi, 0), (\pi, 0, \pi), (0, \pi, \pi)$ . For other  $\mathbf{Q}$ , the values of the SSF should be almost zero or hardly show any size dependence. Indeed, this behavior is confirmed in our calculation. In Fig. 2, we show the results for the field dependence of  $S(\mathbf{Q}_{\text{sol}})$  and  $\rho_s$  at  $(J_\perp, J_z) = (0.2, -1.0)J$  ( $J > 0$ ) and  $k_B T = 0.1J$ . Note that these values of  $J_\perp$  and  $J_z$  denote the ferromagnetic (attractive) hopping and the antiferromagnetic (repulsive) interactions, respectively. The  $H$ -axis can be divided into four regions according to the behaviors of  $S(\mathbf{Q}_{\text{sol}})$  and  $\rho_s$ ; (I) the low-field region  $0 < H < H_{\text{solid1}} \sim 1.15J$ , (II) the lower-intermediate region  $H_{\text{solid1}} < H < H^* \sim 2.2J$ , (III) the upper-intermediate region  $H^* < H < H_{\text{solid2}} \sim 3.1J$ , and (IV) the high-field region  $H_{\text{solid2}} < H$ , where  $H_{\text{solid1}}$ ,  $H^*$ , and  $H_{\text{solid2}}$  are temperature-dependent transition fields. In two regions I and IV, the static structure factor  $S(\mathbf{Q}_{\text{sol}})$  increases in proportion to the system size  $N = L^3$ . Such system-size dependence means the existence of the crystalline order

in the ground state. On the other hand,  $S(\mathbf{Q}_{\text{sol}})$  takes the almost same values regardless of the system size in the region II. This indicates that no crystalline order exists in this region.

The superfluid density  $\rho_s$  is almost zero in the region I. When  $H$  increases, it discontinuously increases at  $H_{\text{solid1}}$  and the system exhibits the superfluidity in the intermediate regions II and III. While  $\rho_s$  scarcely shows the field dependence in the lower intermediate region II, it gradually decreases as  $H$  increases in the upper intermediate region III. The superfluidity in the ground state disappears in the region IV.

Judging from these results for the field dependence of  $S(\mathbf{Q}_{\text{sol}})$  and  $\rho_s$ , the ground state is the normal solid state in the regions I and IV. Since the magnetization plateaus at  $m = 0$  and  $1/4$  appear in the corresponding fields as shown in Fig. 3, these solid phases correspond to the AB and  $A_3B$  ordered phases, respectively. In the region II,  $\rho_s$  and  $S(\mathbf{Q}_{\text{sol}})$  shows the typical feature that  $\rho_s$  takes non-zero values without the system-size dependence of  $S(\mathbf{Q}_{\text{sol}})$ . Consequently, there appears the superfluid state in the ground state. In the region III,  $S(\mathbf{Q}_{\text{sol}})$  shows the system-size dependence with non-zero values of  $\rho_s$ : The crystalline order and the superfluidity coexist. Hence, we conclude that the supersolid state exists and is stable in three dimensions.

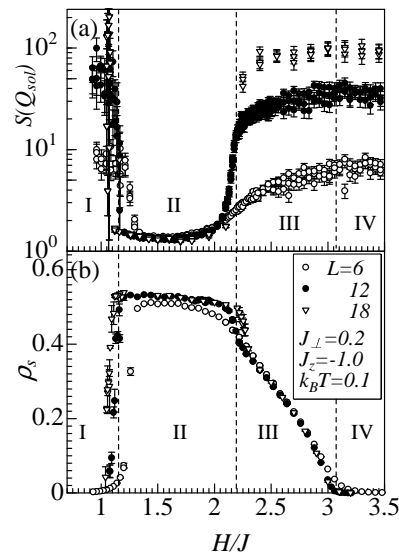


FIG. 2: The field dependence of  $S(\mathbf{Q}_{\text{sol}})$  and  $\rho_s$  at  $(J_\perp, J_z) = (0.2, -1.0)J$  and  $k_B T = 0.1J$ . The open circles, the solid circles, and the inverted triangles denote the results for  $L = 6$ , 12, and 18, respectively.

In order to clarify the finite temperature transition into the supersolid state, we continue to study the temperature dependence of  $S(\mathbf{Q}_{\text{sol}})$  and  $\rho_s$ . The results at  $H = 2.7J$  are shown in Fig. 4. At  $H = 2.7J$ ,  $S(\mathbf{Q}_{\text{sol}})$  almost discontinuously increases at  $k_B T = k_B T_{\text{solid}} \sim 0.32J$  and the system-size dependence appears for  $T < T_{\text{solid}}$ . However, the superfluid density remains in the small values

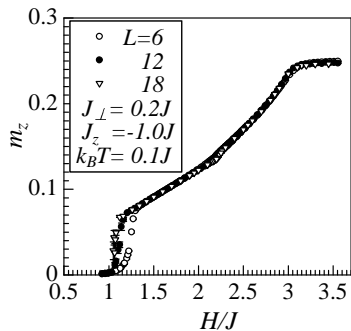


FIG. 3: The field dependence of the magnetization at  $(J_{\perp}, J_z) = (0.2, -1.0)J$  and  $k_B T = 0.1J$ . The value of  $m_z = 0.25$  corresponds to a half of the saturation magnetization.

of  $\rho_s < 5 \times 10^{-3}$  near  $T_{\text{solid}}$ . This behavior is characteristic to the first order transition from the normal fluid phase to the normal solid phase. Since the system-size dependence of  $S(\mathbf{Q}_{\text{sol}})$  shows the same behavior as that in the  $A_3B$  phase, this solid phase corresponds to the  $A_3B$  ordered phase in the region IV.

In the lower-temperature region  $T < T_{\text{solid}}$ , the superfluid density  $\rho_s$  starts increasing at  $k_B T_{\text{super}} \sim 0.22J$ , where the phase transition from the solid state to the supersolid state takes place. To estimate  $T_{\text{super}}$  and identify the universality class of the phase transition, we analyze the finite-size scaling behavior of the helicity modulus  $\Upsilon$ [25] by the scaling form  $\Upsilon L = f(L^{1/\nu}(T - T_{\text{super}}))$ . The results for the system size  $L = 6, 12,$  and  $18$  are plotted in Fig. 4(b). As shown in the inset, the finite-size scaling behavior of  $\Upsilon$  can be explained by the exponents of the three dimensional  $XY$  model[26]. The data collapse is obtained with  $\nu = 0.6723$ [26] when we estimate the critical temperature as  $k_B T_{\text{super}} \sim 0.221(2)J$ . Thus, we conclude that the phase transition from the solid phase to the supersolid phase is of the second order and the universality class is the same as that of three dimensional  $XY$  model.

Using the same analysis, we estimate the critical temperatures  $T_{\text{solid}}$  and  $T_{\text{super}}$  for various  $H$  in order to determine the phase boundary. Here,  $T_{\text{solid}}$  and  $T_{\text{super}}$  denote the transition temperatures where the crystalline order and the superfluid order emerge, respectively. The results are shown in Fig. 5.

In the region  $H > 2.5J$ , the  $A_3B$  crystalline order appears at a higher temperature than the superfluidity. On the contrary, in the region  $H < 2.5J$ , the superfluidity appears at a lower temperature than the crystalline order. However, there are no signs of the phase transition at  $H \sim 2.5J$  in the field dependence of  $S(\mathbf{Q}_{\text{sol}})$  or  $\rho_s$ . Therefore these supersolid phases constitute a single phase.

From the phase diagram in Fig.5, we find that the supersolid phase exists between the AB and  $A_3B$  solid phases. This region locates slightly above  $H_{\text{Ising}} = 2.0J$  where the phase transition occurs from the AB phase to

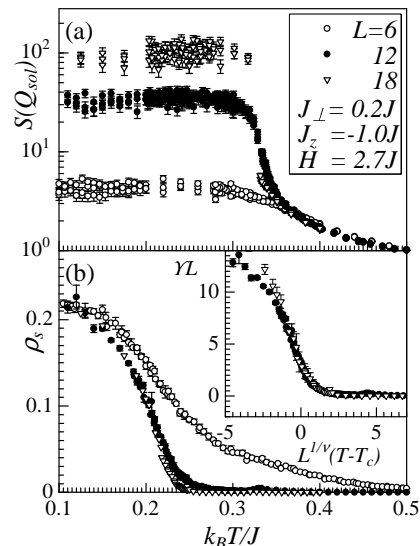


FIG. 4: The temperature dependence of  $S(\mathbf{Q}_{\text{sol}})$  and  $\rho_s$  in  $(J_{\perp}, J_z) = (0.2, -1.0)J$  and  $H = 2.7J$ . The inset in (b) is the finite-size scaling of the helicity modulus. The open circles, the solid circles, and the inverted triangles denote the results for  $L = 6, 12,$  and  $18$ .

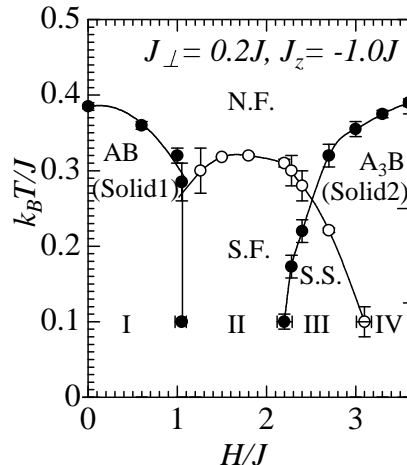


FIG. 5: The phase diagram in  $H$ - $T$  plane for  $(J_{\perp}, J_z) = (0.2, -1.0)J$ . The open circles and the solid circles denote the locations of the first-order ( $T_{\text{solid}}$ ) and the second-order transition ( $T_{\text{super}}$ ), respectively. The solid lines are to guide the eye. "N.F.", "S.F.", and "S.S." mean the normal fluid phase, the superfluid phase, and the supersolid phase, respectively.

the  $A_3B$  phase in the case of  $J_{\perp} = 0$  (Ising model). To discuss the mechanism of the supersolid state on the FCC lattice, we consider the spin configuration above  $H_{\text{Ising}}$ . Slightly above  $H_{\text{Ising}}$  in the Ising model, *dangling* spins (i.e., the spins that can be reversed without changing the energy) appear at the centers of faces of the cubic lattice due to the frustrated interactions and the applied fields. In Fig. 1(b), the locations of the up spins are those of

*dangling* spins. In the region  $H_{\text{Ising}} < H$ , the down-spins at these locations are regarded as hard-core particles that carry the super current. The vacuum at the dangling-spin locations corresponds to the  $A_3B$  solid state. In the region III, particles at the dangling-spin locations can hop to the nearest-neighbor sites and give rise to the super flow when the transverse interaction  $J_{\perp}$  exists. In contrast, for the particles at the corners, it is hard to hop because the gain of the kinetic energy is smaller than the repulsive interaction between the nearest-neighbor particles. Therefore, they constitute the crystalline order. As we decrease the magnetic field that suppresses the creation of particles (down spins), the density of particles increases at the dangling-spin locations, which generate positive molecular fields at the corners, destabilizing the crystalline order. At  $H = H_{\text{Ising}} (\sim H^*)$ , this destabilizing effect finally melts the crystal. This is the microscopic picture for the supersolid above  $H_{\text{Ising}}$ . Especially, the supersolid state in the region  $H_{\text{Ising}} < H$  can be regarded as the  $A_3B$ -type supersolid state because  $S(\mathbf{Q}_{\text{sol}})$  in the regions III and IV takes almost the same value when the temperature  $T$  is fixed. In addition, we have observed the  $A_3B$ -type spin configurations in snapshots of the Monte Carlo simulation.

In the region  $H < H_{\text{Ising}}$ , the emergence of the supersolid of another type, which we could call AB-type, is expected. The mechanism of the AB-type supersolid is also explained by the locations of the *dangling* spins. Slightly below  $H_{\text{Ising}}$ , the down spins in the AB solid state (Fig.1(a)) become dangling and construct the super-flow paths, while the up spins construct the crystalline order. In this case, the superfluid layers and the solid layers are

stacked along one of the orthogonal axes in the AB-type supersolid. The AB-type supersolid has the two dimensional paths of the superfluid, while the  $A_3B$ -type supersolid has the three dimensional superfluid connections. Perturbatively, the effective interactions between these superfluid layers arise in the second order of  $J_{\perp}$ . Therefore, near the phase transition temperature of the AB-type supersolid, a strong cross-over behavior from the two dimensional Kosterlitz-Thouless type to the three-dimensional XY type may be observed as the transverse interaction  $J_{\perp}$  is increased.

The difference between the AB-type and  $A_3B$ -type supersolid may cause the difficulty in observing the AB-type supersolid phase. In our results at  $(J_{\perp}, J_z) = (0.2, -1.0)J$ , a clear evidence for the AB-type supersolid could not be obtained. However the supersolid phase in the classical AB phase may exist near  $H \sim H_{\text{solid1}}$  when  $J_{\perp}$  takes the smaller values. Actually, the existence of the AB-type supersolid is confirmed in our preliminary computation for  $(J_{\perp}, J_z) = (0.15, -1.0)J$  at  $k_B T = 6.67 \times 10^{-2}J$ , which will be reported elsewhere.

To summarize, we have calculated the SSF and the superfluid density for  $S = 1/2$  XXZ model on the FCC lattice and obtained a phase diagram at fixed  $J_{\perp}/J_z$ . We have pointed out that the connections of *dangling* spins resulting from the geometrical frustration play a key role in the formation of the supersolid state.

We would like to thank K. Harada and C. Batista for useful comments and fruitful discussions. Numerical computations were carried out at the facilities of the Supercomputer Center, Institute for Solid State Physics, University of Tokyo.

- 
- [1] O. Penrose and L. Onsager, Phys. Rev. **104**,576 (1956).
  - [2] A. F. Andreev and I. M. Lifshitz, Sov. Phys. JETP **29**, 1107 (1969).
  - [3] G. Chester, Phys. Rev. A **2**, 256 (1970).
  - [4] A. J. Leggett, Phys. Rev. Lett. **25**, 1543 (1970).
  - [5] H. Matsuda and T. Tsuneto, Prog. Theor. Phys. **46**, 411 (1970).
  - [6] M. Liu, Phys. Rev. B **18** 1165 (1978).
  - [7] E. Kim and M. H. W. Chan: Nature **427** (2004) 225; Science **305**, 1941 (2004).
  - [8] A. Griesmaier, J. Werner, S. Hensler, J. Stuhler, and T. Pfau, Phys. Rev. Lett. **94**, 160401 (2005).
  - [9] S. Wessel and M. Troyer, Phys. Rev. Lett. **95**, 127205 (2005).
  - [10] D. Heidarian and K. Damle, Phys. Rev. Lett. **95**, 127206 (2005).
  - [11] R. G. Melko, A. Paramekanti, A. A. Burkov, A. Vishwanath, D. N. Sheng, and L. Balents, Phys. Rev. Lett. **95**, 127207 (2005).
  - [12] M. Boninsegni and N. Prokof'ev, Phys. Rev. Lett. **95**, 237204 (2005).
  - [13] A. A. Burkov and L. Balents, Phys. Rev. B **72**, 134502 (2005).
  - [14] G. Murthy, D. Arovas, and A. Auerbach, Phys. Rev. B, **55**, 3104 (1997).
  - [15] A. Kuklov, N. Prokof'ev, and B. Svistunov, Phys. Rev. Lett., **93**, 230402 (2004).
  - [16] G. G. Batrouni and R. T. Scalettar, Phys. Rev. Lett., **84**, 1599 (2000).
  - [17] S. V. Isakov, S. Wessel, R. G. Melko, K. Sengupta, and Y. B. Kim, Annals. Phys. **321**, 1528 (2006).
  - [18] K. Sengupta, S. V. Isakov, and Y. B. Kim, Phys. Rev. B **73**, 245103 (2006).
  - [19] A. W. Sandvik, Phys. Rev. B **59**,R14157 (1999).
  - [20] K. Harada, cond-mat/0608099.
  - [21] K. Binder, J. L. Lebowitz, M. K. Phani, and M. H. Kalos, Acta Metall **29**, 1655 (1981).
  - [22] H. Meirovitch, Phys. Rev. B **30**, 2866 (1984).
  - [23] S. Kämmerer, B. Dünweg, K. Binder, and M. d'Onorio de Meo, Phys. Rev. B **53**, 2345 (1996).
  - [24] E. L. Pollock and D. M. Ceperley, Phys. Rev. B **36**, 8343 (1987).
  - [25] M. E. Fisher, M. N. Barber, and D. Jasnow, Phys. Rev. A **8**, 1111 (1973).
  - [26] M. Hasenbusch and T. Torok, J. Phys. A: Math. Gen. **32**, 6361 (1999).